Discriminating orthogonal single-photon images

Curtis J. Broadbent,[1] Petros Zerom,[2] Heedeuk Shin,[2] John C. Howell,[1] and Robert W. Boyd[1,2]
[1]*Department of Physics and Astronomy, University of Rochester, Rochester, New York 14627, USA*
[2]*Institute of Optics, University of Rochester, Rochester, New York 14627, USA*
(Received 14 July 2008; published 4 March 2009)

We can encode an image from an orthogonal basis set onto a single photon from a downconverted pair via the use of an amplitude mask. We can then discriminate the image imprinted on the photon from other images in the set using holographic-matched filtering techniques. We demonstrate this procedure experimentally for an image space of two objects, and we discuss the possibility of applying this method to a much larger image space. This process could have important implications for the manipulation of images at the quantum level.

DOI: 10.1103/PhysRevA.79.033802 PACS number(s): 42.30.−d, 42.50.Ex

An individual photon constitutes the basic information carrier in any optical-communication or quantum-information-processing system. Many protocols for encoding information onto an optical beam limit the information content of each photon to one bit of information, or to one qubit of information for quantum protocols. However, recent work has emphasized the vast Hilbert space and thus the vast potential information content of a single photon. One such example [1–3] is the use of the orbital angular-momentum states, such as Laguerre-Gauss states, of the photon. These states form an infinite basis, implying that in principle there is no limit to the information content that can be carried by a single photon. Other examples of the large information content of quantum light field exist as well [4–7]. For example, entanglement of a large number of photons, of the order of 100, has been demonstrated [8]. Moreover, it has recently been shown that the entanglement between two photons generated by the process of parametric down conversion can exist in a high-dimensional Hilbert space; entanglement between two qudits was demonstrated for both $d=3$ and $d=6$ with transverse position-momentum entangled biphotons [9], and $d=1024$ with energy-time entangled biphotons [10].

In this paper, we describe an experimental procedure that we have used to impress transverse image information onto an individual photon. If the image is a member of a preestablished basis set, we can determine which image is carried by the photon by performing a single measure. This procedure should be contrasted with the earlier work of [11], in which an image was impressed upon a single photon, but the image was read out in a statistical fashion, one pixel at a time, and thus required an ensemble of events to reproduce the image. That work also established that the individual photons carrying the image could be delayed significantly by passing them through a highly dispersive (slow-light) medium without destroying the image content of the photon.

The basic idea of our approach is illustrated in Fig. 1. We first form a multiple-exposure hologram (parts a and b) using two different transmission objects with reference beams applied from different directions. We then (part c) pass a single photon through one of the two objects and allow it to fall onto the hologram constructed by the procedure shown in parts (a) and (b). This photon will then diffract into one of two output directions depending upon which image was impressed onto the photon. This procedure is well known in optical information processing [12,13] and is related to the more general method of matched filtering [14]. The general methods used in classical image discrimination apply equally well to quantum-mechanical light fields. Whereas Mair *et al.* [1] used simplex holograms to measure single-photon orbital angular-momentum states, the present work demonstrates that arbitrary image states from a known basis set may be distinguished by performing a single measure with a multiplexed hologram. In the conceptual example shown in Fig. 1, our basis set consists of only two images. We present results from a proof-of-principle experiment which distinguishes between two orthogonal images. However, much larger sets of images (orthogonal or nonorthogonal) can be used. In the classical field of matched filtering, as many as 10 000 images have been exposed onto a single hologram [15].

A schematic of our experimental setup is shown in Fig. 2. Part (a) shows the setup for writing the hologram and part (b) shows the setup for the single-photon readout. For this experiment, we use stencils of yin and yang symbol as objects A and B, respectively. We choose these objects because they have vanishing spatial overlap and in this sense constitute orthogonal objects. The hologram is a thick angularly multiplexed phase transmission hologram and is made using PFG-

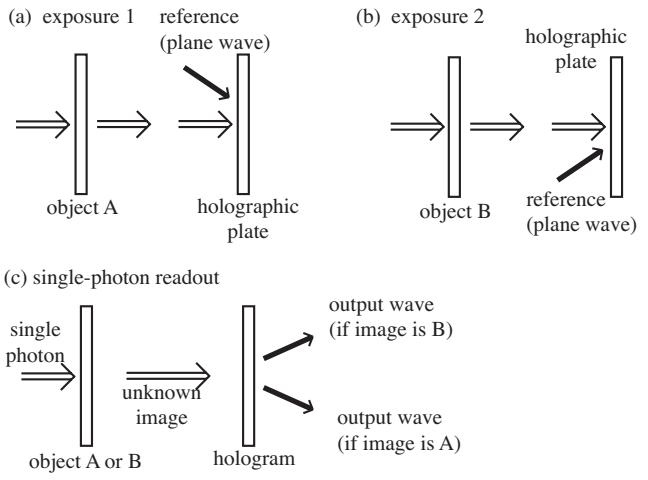

FIG. 1. Concept of the experiment. A multiple-exposure hologram (shown for two exposures) is formed as shown in parts (a) and (b) of the figure. (c) An image is impressed onto a single photon and the form of the image is determined by diffraction from the hologram.

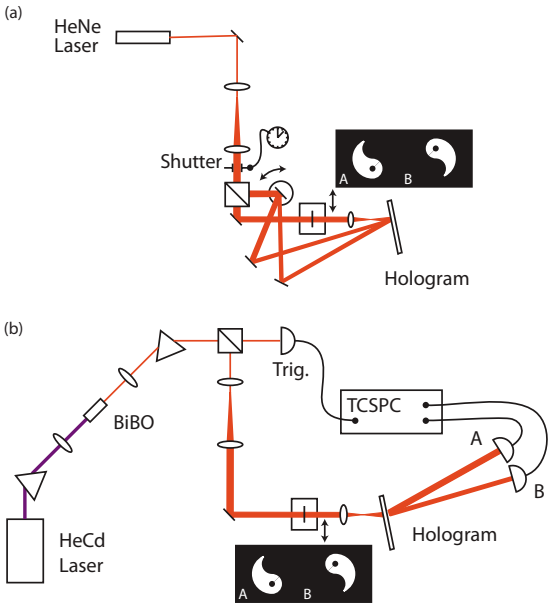

FIG. 2. (Color online) Single-photon image-discrimination laboratory setup. (a) Biplex holograms are exposed using a HeNe laser and an electronically controlled shutter. For each exposure a rotation stage selects one of the two reference beams, and a translation stage switches between the two stencils A and B. (b) During the image-discrimination phase of the experiment, heralded single photons are sent through either stencil A or B and are detected at either detector A or B. TCSPC=time-correlated single-photon counter.

01, a fine-grained red-sensitive silver halide emulsion on a glass plate substrate [16]. The emulsion has a peak light sensitivity of about 100 μJ/cm^2 at 630 nm.

We use a HeNe laser (λ=632 nm) as the light source for recording the holograms. The HeNe laser is split at a nonpolarizing beamsplitter (NPBS) into object and reference beams. Each beam has a power of ~300 μW after the NPBS. The object beam passes through the object stencil and is imaged onto the hologram recording medium with a 50 mm focal length lens, along with one of the two reference beams. A precision translation stage allows us to reproducibly place either object A or B in the object plane. The reference beam is sent to a mirror mounted on a rotation stage which sets the direction of the reference beam. During the exposure, object A (B) is illuminated and the hologram is exposed with reference beam A (B) for 350 ms as set by an electronically controlled shutter.

We have characterized the performance of these holograms. Parts (a) and (b) of Fig. 3 show the quality of the reconstructed images when the hologram is read out by a plane-wave reference beams. Parts (c) and (d) show the diffracted beams when the hologram is illuminated by one of the image-bearing beam. The nature of these results is described by a model of the holographic process. We assume that the holographic recording material is illuminated simultaneously by an object wave of field strength $O(\mathbf{x})$ and a reference wave of field strength $R(\mathbf{x})$ so that the total field at the hologram is $E(\mathbf{x})=O(\mathbf{x})+R(\mathbf{x})$. We assume that after development, the transmission $t(\mathbf{x})$ of the hologram is proportional to the local optical intensity so that $t(\mathbf{x})\propto|O(\mathbf{x})+R(\mathbf{x})|^2$ or that

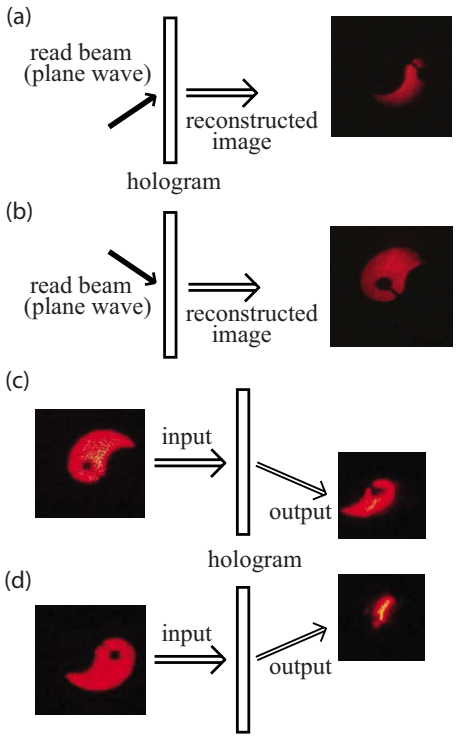

FIG. 3. (Color online) (a) and (b) Hologram readout for a plane-wave read beam. (c) and (d) Hologram readout with an image-carrying read beam.

$$t(\mathbf{x}) \propto |O(\mathbf{x})|^2 + |R(\mathbf{x})|^2 + O(\mathbf{x})R^*(\mathbf{x}) + O^*(\mathbf{x})R(\mathbf{x}). \quad (1)$$

In the conventional holographic reconstruction process, the hologram is illuminated with a wave identical to the reference wave $R(\mathbf{x})$ used in writing the hologram so that the field leaving the hologram is given by $E_{\text{out}}(\mathbf{x})\propto R(\mathbf{x})t(\mathbf{x})$ or by

$$R(\mathbf{x})|O(\mathbf{x})|^2 + R(\mathbf{x})|R(\mathbf{x})|^2 + O(\mathbf{x})|R(\mathbf{x})|^2 + O^*(\mathbf{x})R^2(\mathbf{x}). \quad (2)$$

The third term in this expression is the one leading to standard holographic reconstruction, and if $R(\mathbf{x})$ is nearly uniform across the aperture of the hologram we see that this term just reproduces the amplitude distribution $O(\mathbf{x})$ of the original object. Such behavior can be seen in parts (a) and (b) of Fig. 3, where the reconstructed images are accurate replicas of the stencil objects. If, however, the hologram is illuminated by a replica of the structured object beam $O(\mathbf{x})$, as in the case of holographic matched filtering, the situation is more complicated. We find that $E_{\text{out}}(\mathbf{x})\propto O(\mathbf{x})t(\mathbf{x})$ or by

$$O(\mathbf{x})|O(\mathbf{x})|^2 + O(\mathbf{x})|R(\mathbf{x})|^2 + O^2(\mathbf{x})R^*(\mathbf{x}) + |O(\mathbf{x})|^2R(\mathbf{x}). \quad (3)$$

In this case, the fourth term is the one leading to the diffracted output beam, and we see that the transverse structure of the object beam will be imprinted onto the diffracted beam. This behavior is apparent in the data shown in parts (c) and (d) of Fig. 3. Quantitatively, we have measured a peak diffraction efficiency of about 24% (19%) for objects A

TABLE I. Image-discrimination results showing the total number of raw coincidences (C), accidental coincidences (A), and C/A ratio for each object-detector combination. Also shown are the heralding photon and image-discrimination photon singles rates, s_h and s_{id}. Background rates are $b_h \simeq 1000 \pm 32$ Hz, $b_{\mathrm{id,A}} = 420 \pm 20$ Hz, and $b_{\mathrm{id,B}} = 249 \pm 16$ Hz. $1/R\Delta t$ represents the maximum possible C/A ratio as discussed in the text.

Object-detector	C	A	C/A	s_h (kHz)	s_{id} (Hz)	$1/R\Delta t$
A - A	5738 ± 75	337 ± 18	16.99 ± 0.95	437	473	143 ± 3
A - B	185 ± 14	201 ± 14	0.93 ± 0.09	522	252	N/A
B - A	289 ± 17	287 ± 17	1.01 ± 0.08	444	414	N/A
B - B	4401 ± 66	229 ± 15	19.24 ± 1.30	511	273	210 ± 5

(B), and we find that the cross talk between them is negligible.

The image-discrimination phase of the experiment is performed with the setup of Fig. 2(b). The object beam is created by heralded single photons emitted by spontaneous parametric downconversion. We angle tune the 10-mm-long BiBO crystal cut for collinear type-I phase matching to produce degenerate biphotons at 650 nm. The biphotons are separated from the pump beam and are sent to a NPBS. One output port of the NPBS is coupled directly through a multimode optical fiber to a photon detector which serves as a trigger, heralding the presence of a photon, hereafter called the image photon, in the other output port. The image photon passes through the stencil and hologram along the same path as when the hologram was exposed. After diffracting from the hologram, the image photons are coupled through multimode fibers to detectors A or B. All three detectors used in the experiment are Perkin-Elmer single-photon counting module (SPCM) detectors. Detection events are counted with a PicoQuant PicoHarp 300, a time-correlated single-photon counter (TCSPC).

When stencil A (B) is used as the object, the image-discrimination photons are diffracted by the hologram into the direction of reference beam A (B). Coincidences between the herald and the image-discrimination photons are measured for the four object-detector combinations: (1) A-A, (2) A-B, (3) B-A, and (4) B-B. The total number of coincidences for 54 min of integration are reported in Table I. For better visualization, these results are also shown graphically in Fig. 4. Raw coincidences are the number of coincident events generated within the 500 ps coincidence window. Coincident events arise from coincidences between the herald and image-discrimination photons as well as random coincident events between (a) a background count and a heralding photon, (b) a background count and an image-discrimination photon, (c) two background counts, or (d) two uncorrelated photons from a multipair event. By counting the number of image-discrimination photons that arrive 20 ± 0.25 ns after the heralding photons we can measure the number of accidental coincidences arising from events (a)–(d) above. The single-event count rates are ~500 k counts/s for the trigger and ~450 counts/s (~250 counts/s) for detector A (B) (see Table I). In practice, the high degree of loss in the image-discrimination arm implies that the accidental coincidences are dominated by coincidences between background counts and heralding photons.

The system fidelity can be quantified in terms of the ratio of true coincidences N_{AA} (N_{BB}) to false coincidences N_{AB} (N_{BA}). The ratio $f_{\mathrm{A}} = N_{\mathrm{AA}}/N_{\mathrm{AB}}$ ($f_{\mathrm{B}} = N_{\mathrm{BB}}/N_{\mathrm{BA}}$) is found to be 31.2 (15.2), demonstrating that object A can be distinguished from B with a confidence level of ~96.8% (93.4%). It is evident from the data in Table I that nearly all of the false events, N_{AB} and N_{BA}, can be attributed to accidental coincidences (because the C/A ratios for the A-B and B-A object-detector combinations are approximately unity). The system fidelity can therefore be increased by improving the C/A ratios for the A-A and B-B object-detector combinations. The C/A ratios can be improved by increasing the total collection efficiency in the image-discrimination arm or by using detectors with reduced dark counts for the image-discrimination photon. The low collection efficiency in the image-discrimination arm is due to a combination of reflection losses at lenses, mirrors and beamsplitters, transmission losses at the image mask and hologram, coupling losses from coupling a highly multimode image into a multimode optical fiber, and alignment issues caused by using different laser wavelengths for the hologram exposure, single-photon generation, and single-photon alignment.

We estimate that by using improved single-photon detectors, such as Perkin-Elmer SPCM-AQR-16 detectors that have only 25 dark counts/s, and by improving the collection efficiency in the image-discrimination arm, a C/A ratio of roughly 150, corresponding to a confidence level of 99.34%,

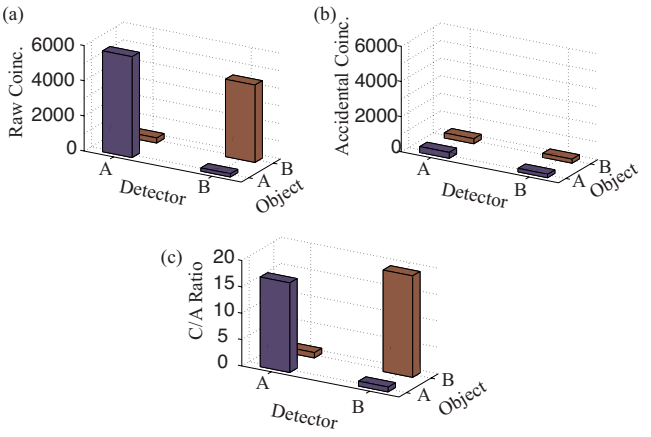

FIG. 4. (Color online) Graphical display of image-discrimination results. Total number of raw coincidences (C), accidental coincidences (A), and C/A ratio for each object-detector combination.

could be achieved for our current experimental setup. Assuming that the count rates are much smaller than the detector inverse dead time, the C/A ratio can be reduced to the following expression:

$$C/A = 1 + \frac{1}{R\Delta t}\left[\left(1 + \frac{b_1}{\epsilon_1 R}\right)\left(1 + \frac{b_2}{\epsilon_2 R}\right)\right]^{-1}, \tag{4}$$

where ϵ_i is the collection and detection efficiency of the ith detector and b_i is the background count rate (detector dark count rate plus stray light count rate) for the ith detector. R is the rate at which photon pairs are emitted by the crystal and Δt is the duration of the coincidence window. In an ideal setting where $b_i \ll \epsilon_i R$, the C/A ratio is limited by $(R\Delta t)^{-1}$ and the discrimination confidence level is limited by $1 - R\Delta t$. In the present experiment $(R\Delta t)^{-1} \sim 143$ so that the discrimination confidence level is bounded by 99.30%. To date, the best C/A ratio in entangled biphoton sources is ~ 1000 from a Raman-scattering process in optical fiber [17].

The work presented here shows that it is possible to impress an image onto an optical field comprised of a single photon and subsequently sort these photons into classes determined by the image that the photon carries. For this initial study, we used basis sets containing only two spatially separated images, for which very good discrimination was obtained with a multiplexed image hologram. For many applications, a much larger basis set, possibly including nonspatially separated, or more generally, nonorthogonal images, would be desirable. Image discrimination of nonorthogonal images using numerical correlation methods has been investigated by [18] where Morris showed that distinguishing images with a confidence level of 97% requires about 250 photons. For a basis set involving nonorthogonal images the principles of unambiguous state discrimination in large Hilbert spaces [19] may be applied to design a hologram which optimally discriminates images in the basis set. Limits to the number of images that can be discriminated in a hologram are set by issues such as cross talk, which tends to increase with the number of stored images, and diffraction efficiency, which tends to decrease with the number of stored images. However, it is reassuring to note that as many as 10 000 images have been stored in a holographic memory under appropriate conditions [15].

This work was supported by the U.S. Army Research Office through a MURI grant.

[1] A. Mair, A. Vaziri, G. Weihs, and A. Zeilinger, Nature (London) **412**, 313 (2001).
[2] G. Molina-Terriza, J. P. Torres, and L. Torner, Phys. Rev. Lett. **88**, 013601 (2001).
[3] J. Leach, J. Courtial, K. Skeldon, S. M. Barnett, S. Franke-Arnold, and M. J. Padgett, Phys. Rev. Lett. **92**, 013601 (2004).
[4] H. de Riedmatten, I. Marcikic, V. Scarani, W. Tittel, H. Zbinden, and N. Gisin, Phys. Rev. A **69**, 050304(R) (2004).
[5] J. T. Barreiro, N. K. Langford, N. A. Peters, and P. G. Kwiat, Phys. Rev. Lett. **95**, 260501 (2005).
[6] S. P. Walborn, D. S. Lemelle, M. P. Almeida, and P. H. Souto Ribeiro, Phys. Rev. Lett. **96**, 090501 (2006).
[7] P. Walther, M. Aspelmeyer, and A. Zeilinger, Phys. Rev. A **75**, 012313 (2007).
[8] H. S. Eisenberg, G. Khoury, G. Durkin, C. Simon, and D. Bouwmeester, Phys. Rev. Lett. **93**, 193901 (2004).
[9] M. N. O'Sullivan-Hale, I. A. Khan, R. W. Boyd, and J. C. Howell, Phys. Rev. Lett. **94**, 220501 (2005).
[10] I. Ali-Khan, C. J. Broadbent, and J. C. Howell, Phys. Rev. Lett. **98**, 060503 (2007).
[11] R. M. Camacho, C. J. Broadbent, I. Ali-Khan, and J. C. Howell, Phys. Rev. Lett. **98**, 043902 (2007).
[12] A. Vander Lugt, Proc. IEEE **62**, 1300 (1974).
[13] G. M. Morris and N. George, Opt. Lett. **5**, 202 (1980).
[14] G. L. Turin, IRE Trans. Inf. Theory **6**, 311 (1960).
[15] X. An, D. Psaltis, and G. W. Burr, Appl. Opt. **38**, 386 (1999).
[16] Our holograms were made using well-established laboratory procedures. See, for instance: P. Hariharan, *Optical Holography* (Cambridge University Press, Cambridge, 1984); R. J. Collier *et al.*, *Optical Holography* (Academic, New York, 1971). The holographic recording material was purchased from Slavich, Vilnius 2006, Lithuania.
[17] J. Fan and A. Migdall, Opt. Express **15**, 2915 (2007).
[18] G. M. Morris, Appl. Opt. **23**, 3152 (1984).
[19] A. Peres and D. R. Terno, J. Phys. A **31**, 7105 (1998).